NASA TN D-139

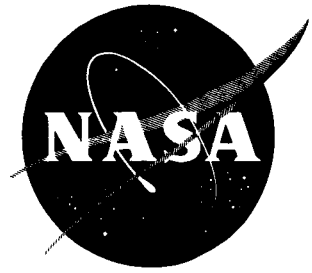

TECHNICAL NOTE
D-139

AN EXPLORATORY INVESTIGATION IN A BALLISTIC RANGE OF THE STABILITY DERIVATIVES OF A SIMPLE AIRPLANE CONFIGURATION AT LOW SUPERSONIC SPEEDS

By Charles E. DeRose and Alfred G. Boissevain

Ames Research Center
Moffett Field, Calif.

NATIONAL AERONAUTICS AND SPACE ADMINISTRATION

WASHINGTON December 1959

NATIONAL AERONAUTICS AND SPACE ADMINISTRATION

TECHNICAL NOTE D-139

AN EXPLORATORY INVESTIGATION IN A BALLISTIC RANGE OF THE STABILITY DERIVATIVES OF A SIMPLE AIRPLANE CONFIGURATION AT LOW SUPERSONIC SPEEDS

By Charles E. DeRose and Alfred G. Boissevain

SUMMARY

An exploratory investigation of the problems of obtaining stability derivatives of airplanelike models in a ballistic range was conducted. A simple body-wing-tail configuration having two planes of mirror symmetry was tested at Mach numbers of 1.2 to 1.4 and Reynolds numbers (based on wing chord) of 0.8 to 1.0×10^6. Results showed that stability derivatives could be extracted only from those runs in which the rolling rate was negligibly small or zero; stability derivatives from these runs compared fairly well with existing theory.

INTRODUCTION

The value of the ballistic range type of test facility for the determination of the stability derivatives of axially symmetric shapes has been demonstrated repeatedly. The chief advantage of this type of facility is that tests can be performed on small-scale restraint-free models at high Mach numbers. Because of the increasing interest in unsymmetrical shapes as vehicles for very high speed flight in the atmosphere, a program has been established at the Ames Research Center to investigate the problems and limitations of determining the stability derivatives of airplanelike (i.e., nonaxially symmetric) configurations in a ballistic range. A similar study made at the Canadian Armament Research and Development Establishment on a series of flat-plate wings of triangular plan form is reported in reference 1.

This report presents the results of tests obtained on a simple body-wing-tail configuration during an early phase of this investigation. The tests were performed in the Ames supersonic free-flight underground range.

SYMBOLS

A,B,C,D E,F,G,H	coefficients in equations of motion
b	wing span, ft
C_{L_α}	lift curve slope, $\frac{\partial L/qS}{\partial \alpha}$
C_{m_α}	pitching-moment curve slope, $\frac{\partial M/qSc}{\partial \alpha}$
$C_{m_{\dot{\alpha}}}$	$\frac{\partial M/qSc}{\partial \dot{\alpha} c/2V}$, per radian
C_{m_q}	$\frac{\partial M/qSc}{\partial qc/2V}$, per radian
C_{Y_β}	side-force curve slope, $\frac{\partial Y/qS}{\partial \beta}$
C_{n_β}	yawing-moment curve slope, $\frac{\partial n/qSb}{\partial \beta}$
$C_{n_{\dot{\beta}}}$	$\frac{\partial n/qSb}{\partial \dot{\beta} b/2V}$, per radian
C_{n_r}	$\frac{\partial n/qSb}{\partial rb/2V}$, per radian
c	wing chord, ft
I_{XX},I_{YY},I_{ZZ}	moments of inertia about the principal axes of model, slug-ft^2
L	lift force, lb
M	Mach number; also pitching moment about center of gravity of model, ft-lb
m	mass of model, slugs
n	yawing moment about center of gravity of model, ft-lb
p	angular velocity about model X axis, radians/sec

q	dynamic pressure, lb/ft^2; also angular velocity about model Y axis, radians/sec
R	Reynolds number based on wing chord and free-stream conditions
r	angular velocity about model Z axis, radians/sec
S	wing area, exposed surface, ft^2
t	time, sec
V	velocity of model with respect to air, ft/sec
X,Y,Z	principal axes, model fixed
$\bar{X},\bar{Y},\bar{Z}$	earth fixed axes - also displacements along these axes
Y	side force, lb
α	angle of attack, radians in equations, degrees in figures
β	angle of sideslip, radians in equations, degrees in figures
φ	angle of roll, radians
θ	pitch angle between model axis and horizontal ($\bar{X}\bar{Y}$) plane, radians
ψ	yaw angle between vertical plane containing the model axis and the vertical ($\bar{X}\bar{Z}$) plane, radians

Subscripts

0	at time 0
t	at time t

Superscripts

$\cdot$	first derivative with respect to time
$\cdot\cdot$	second derivative with respect to time

FACILITY AND MODELS

Tests were conducted in the Ames supersonic free-flight underground range in which a 3-inch smooth bore, powder-driven gun was used to launch the models into free flight at transonic speeds. The models, of the configuration shown in figure 1, then flew along an instrumented course. Figure 2 shows representative shadowgraphs of the models in flight. The range, located within a concrete shell 7 feet square, has a test section length of 67 feet with seven observation stations. Each station takes two orthogonal shadowgraph pictures, as is indicated in figure 3. The light screen shown in this figure is part of a photoelectric triggering device to actuate the sparks. Reference marks are recorded on the film to permit the determination of the model's spatial and angular orientation. The projection of the angle of pitch was measured on the side film relative to a vertical plumb-bob wire, and the vertical displacement was measured parallel to that wire. A multilegged mercury manometer with a visible tube end in each station was used to establish a height reference. The angle of yaw and sideways displacement were measured in a similar manner on the bottom film with a taut wire stretched the length of the range as a reference. The intervals of time between the firings of the spark units at adjacent stations were recorded on commercial 1.6 megacycle counters.

The models were made from aluminum and brass in four sections. The body was machined from aluminum with a brass nose section pressed on to move the center of gravity forward. The tail section was machined from a solid block of aluminum and pressed into a slot cut into the body. Steel pins were used to secure the wings and tail sections to the body. Table I lists the mass characteristics of the three models used for the data in this report.

The sabot used for launching this model consisted of a steel-faced hollow plastic cup with a set of four foamed-plastic fingers for model alinement. A photograph showing the model and a partially assembled sabot is shown in figure 4. The alining fingers were crushed down to size and final shape on being loaded into the gun.

ACCURACY

The determination of accuracy of measurement of the stability derivatives was an objective of this investigation and could not be predicted beforehand. However, an estimate can be made of the accuracy of determining stability derivatives of a model with linear variation of aerodynamic characteristics experiencing a planar oscillation. In this facility, the position of the model in space relative to range axes was determined to within 0.005 inch and the angular orientation was measured to 0.05°. Time is accurate to ± 0.6 microsecond. With this precision of measurement, the percent accuracy of stability coefficients is as follows:

C_{l_α}	±3
C_{m_α}	±2
C_{Y_β}	±6
C_{n_β}	±4
$(C_{m_q} + C_{m_{\dot{\alpha}}})$	±25
$(C_{n_r} - C_{n_{\dot{\beta}}})$	±25

The uncertainty of model dimensions is extremely small and is believed to have a negligible effect on the data.

ANALYSIS

The basic data from the free-flight tests consist of time histories of the angular orientation and displacement of the model's axes with respect to fixed earth axes. The angles and displacements are defined in figure 5(a). It should be noted that only the angle of yaw ψ, is measured directly from the film. The angle recorded on the side-station film is the angle between the $\bar{X}$ axis and the projection of the model's X axis on the $\bar{X}\bar{Z}$ plane. For values of ψ encountered, the measured angle and the angle θ are effectively equal. Figure 5(b) shows the relationship between the velocity vector and the model axes. The figure shows a three-dimensional representation of the significant vectors and, in the insert, a projection on the $\bar{Y}\bar{Z}$ plane. At any given station the angle of attack, α, and of sideslip, β, can be determined using the relationships defined in figure 5(b).

$$\alpha = (\theta+\dot{\bar{Z}}/V)\cos\varphi + (\psi-\dot{\bar{Y}}/V)\sin\varphi \tag{1}$$

$$\beta = -(\psi-\dot{\bar{Y}}/V)\cos\varphi + (\theta+\dot{\bar{Z}}/V)\sin\varphi \tag{2}$$

The complete differential equations of motion for a body rolling at a constant rate have been developed by a number of authors (e.g., ref. 2) and can be expressed in the form shown below. These equations are referred to the principal axes of the model and are based on the assumptions of linear coefficients with no aerodynamic cross-coupling, controls fixed, and four degrees of freedom (constant roll rate and zero change in forward velocity).

$$\ddot{\alpha} + A\dot{\alpha} + B\alpha + C\dot{\beta} + D\beta = 0 \tag{3}$$

$$\ddot{\beta} + E\dot{\beta} + F\beta + G\dot{\alpha} + H\alpha = 0 \tag{4}$$

where the coefficients are defined as follows:

$$A = \frac{C_{L_\alpha} qS}{mV} - \frac{qSc^2}{2VI_{YY}} (C_{m_q} + C_{m_{\dot{\alpha}}})$$

$$B = -\frac{C_{m_\alpha} qSc}{I_{YY}} - \frac{(qSc)^2}{2mV^2 I_{YY}} C_{m_q} C_{L_\alpha} + \frac{I_{XX}-I_{ZZ}}{I_{YY}} p^2$$

$$C = -p\left(\frac{I_{XX}-I_{ZZ}}{I_{YY}} - 1\right)$$

$$D = -p\left(\frac{qSc^2}{2VI_{YY}} C_{m_q} - \frac{I_{XX}-I_{ZZ}}{I_{YY}} C_{Y_\beta} \frac{qS}{mV}\right)$$

$$E = -\frac{C_{Y_\beta} qS}{mV} - \frac{qSb^2}{2VI_{ZZ}} (C_{n_r} - C_{n_{\dot{\beta}}})$$

$$F = \frac{C_{n_\beta} qSb}{I_{ZZ}} + \frac{(qSb)^2}{2mV^2 I_{ZZ}} C_{n_r} C_{Y_\beta} - \frac{I_{YY}-I_{XX}}{I_{ZZ}} p^2$$

$$G = -p\left(1 + \frac{I_{YY}-I_{XX}}{I_{ZZ}}\right)$$

$$H = p\left(\frac{qSb^2}{2VI_{ZZ}} C_{n_r} - \frac{I_{YY}-I_{XX}}{I_{ZZ}} C_{L_\alpha} \frac{qS}{mV}\right)$$

The coefficients C, D, G, and H and a part of the coefficients B and F are functions of the roll rate and are the terms which change the α and β excursions from the form of a damped sine wave to a more complicated form. It was felt that if a damped sine wave could be fitted to the data for α and β, the effects of rolling velocity could be considered negligible; conversely, if the form of the data were in a more complicated curve, then the effects of rolling velocity would be significant. Figure 6(a) shows the variation of α and β with time for a run in which the rolling-velocity effects were not important and figure 6(b) shows data from a run in which rolling-velocity effects were important. Although seven stations were available, not all operated during a given run, and both runs shown have one station missing.

For the runs in which rolling-velocity effects were significant, the coupled equations (3) and (4) apply. An analog computer was utilized in an effort to determine the values of the six coefficients and initial conditions that define the motion. Note that with the roll rate known from measurements, the coefficients C and G are known. A simplified diagram of the computer arrangement is shown in figure 7. The coefficients of the equations and the initial values of the angles and angular rates

appear as potentiometer settings. The equation would be considered solved if the trajectory printed by the computer matched the observed trajectory in the range.

For runs in which the roll rate, p, was zero or could be neglected, the two differential equations of motion are independent and are subject to analytical solution. Equations (3) and (4) become, with $p = 0$:

$$\ddot{\alpha} + A\dot{\alpha} + B\alpha = 0 \tag{5}$$

$$\ddot{\beta} + E\dot{\beta} + F\beta = 0 \tag{6}$$

the solutions of which are:

$$\alpha = e^{-(A/2)t}\left(\alpha_o \cos\ \omega_1 t + \frac{A\alpha_o + 2\dot{\alpha}_o}{2\omega_1} \sin\ \omega_1 t\right) \tag{7}$$

$$\beta = e^{-(E/2)t}\left(\beta_o \cos\ \omega_2 t + \frac{E\beta_o + 2\dot{\beta}_o}{2\omega_2} \sin\ \omega_2 t\right) \tag{8}$$

where

$$\omega_1 = \sqrt{B - A^2/4} \qquad \omega_2 = \sqrt{F - E^2/4}$$

and where A, B, E, and F are the coefficients defined previously with p set equal to zero. Note that these solutions apply only when ω_1 and ω_2 are real. The values of the coefficients are adjusted to provide a best fit to the observed variation of the angular displacement using a least-squares procedure. An inspection of the definition of the coefficients B and F shows that the stability derivatives C_{m_α} and C_{n_β} are not uniquely defined by an evaluation of B and F. Fortunately, the second term in both of these expressions is, for most cases, extremely small relative to the first, and can safely be ignored. The determination of the damping derivatives $(C_{m_q} + C_{m_{\dot{\alpha}}})$ and $(C_{n_r} - C_{n_{\dot{\beta}}})$ from the coefficients A and E is dependent on the prior evaluation of C_{L_α} and C_{Y_β} by the method outlined below.

Force measurements are obtained by relating the displacement of the model's center of gravity to the model's angular displacement. The longitudinal differential equation of displacement can be written

$$C_{L_\alpha}\alpha qS = -m\ddot{Z} \tag{9}$$

if it is assumed C_L is 0 for $\alpha = 0$. The expression for α from equation (7) may be substituted into equation (9) which is then integrated twice with respect to time as indicated in equation (10).

$$-(Z_t-Z_o) + \dot{Z}_o t = qS/m\, C_{L_\alpha} \int_o^t \int_o^t e^{-(A/2)t}\left(\alpha_o \cos \omega_1 t + \frac{A\alpha_o + 2\dot{\alpha}_o}{2\omega_1} \sin \omega_1 t\right) dt\, dt \tag{10}$$

The double integral on the right side of equation (10) can be evaluated since both the integrand and the limits are known.

In a similar manner C_{Y_β} is obtained from the recorded variation of lateral displacement, Y.

RESULTS AND DISCUSSION

This investigation was primarily directed at determining whether stability derivatives could be successfully obtained from airplane models in ballistic range tests. Therefore, in this section the degree of success obtained and the limitations and problems encountered in determining the derivatives from the basic test data will be discussed. In addition, stability data obtained will be presented and compared with theory. Two classes of flight trajectories will be considered; those for which the effects of rolling velocity are negligible and those for which the effects are significant.

Rolling Velocity Effects Negligible

With the stringent requirement of negligible roll effects, three runs, numbers 8, 15, and 16, were found to have sufficient pitching or yawing amplitude to permit an analysis. Figure 8 shows the basic time-history records of these runs. The values of C_{Y_β} and C_{n_β}, and C_{L_α} and C_{m_α} obtained from these runs are plotted in figures 9 and 10, respectively, and are compared to theoretical results computed by the method of reference 3. As can be seen, the experimental data in the lateral plane (C_{Y_β} and C_{n_β}) are in fairly good agreement with the theoretical values. Figure 10 shows that with the exception of the stability derivative C_{m_α} for run 8 the longitudinal characteristics are in fairly good agreement with the theory of reference 3. The failure of the method of reference 3 to predict C_{m_α} for run 8 results from the fact that this method does not account for the effect of sideslip on the aerodynamic interference on the tail surfaces due to the wing flow field. Estimates of this effect have been made for run 8 and the addition of this correction brings the theoretical estimate into better agreement with the experimental value. The effect of sideslip on C_{L_α} for the run is small and is not indicated on the plot.

Figure 11 shows the values of the damping derivatives $(C_{m_q} + C_{m_{\dot{\alpha}}})$ and $(C_{n_r} - C_{n_{\dot{\beta}}})$ obtained from the experimental data compared with theoretical results based on the methods of reference 4. The results from run 8 show good agreement with theory, while runs 15 and 16 show about twice as much damping. It should be noted that the definition of the latter two oscillations is not as good as it is in the case of run 8. An inspection of the plots of the angular time-histories of these runs (fig. 8) shows that a small shift in the location of the t axis, corresponding to a small trim angle, would seriously affect the ratio of peak amplitudes. Increased confidence in the dynamic derivatives would be obtained by the use of a longer instrumented range with more stations.

Rolling Velocity Effects Significant

The method of data analysis utilizing the analog computer failed to yield satisfactory results. Although considerable time was spent adjusting the potentiometer settings, it was not possible to obtain a satisfactory fit to the observed trajectory. Figure 12 represents the best fit obtained from all runs attempted. Although this fit looks fairly good, the potentiometer settings, when translated into aerodynamic coefficients, were not consistent with either theoretical values or with experimental data from nonrolling flights. If potentiometer settings, calculated from estimated aerodynamic coefficients, were used, the fit seemed to be poorer than that of figure 12.

From this experience, it was concluded that the analog computer could not be used to compute aerodynamic coefficients from rolling flights of this length. The reason for this failure is not completely known but various theories can be advanced. First, because every quantity in the analog network is changed by the adjustment of a single potentiometer, it is seen that the procedure is extremely sensitive to each individual part. Therefore, if all potentiometers are not correct at one time, the trajectory will be hopelessly incorrect. Thus, any method of "homing in" on the correct settings would be extremely tedious if not impossible. Secondly, the flight trajectories from this investigation were relatively short. A fairly good match to a trajectory of this length might be totally unacceptable if additional range data were available. For example, at the end of the known trajectory in figure 12, the analog trace for α is beginning to diverge from the faired data. It is probable that a poor fit to a longer trajectory, yet one that agreed generally with the data over many cycles, would provide a better definition of the unknowns in the equations of motion than an exact fit to a shorter run containing only a cycle or so.

CONCLUDING REMARKS

Tests were conducted on an airplanelike model in a seven station ballistic range. On the basis of these tests it was found that reduction of data from model flights during which the effects of rolling velocity were negligible was straightforward and yielded static-stability derivatives that compared fairly well with theoretical values. The agreement of dynamic derivatives with theory would have been improved if a longer instrumented range with more stations had been used. An analog computer analysis of the trajectories of model flights in which rolling-velocity effects were significant failed to yield usable results.

Ames Research Center
National Aeronautics and Space Administration
Moffett Field, Calif., Aug. 25, 1959

REFERENCES

1. Tidy, G. H., and Thomas, Miss M. E.: Canadian Armament Research and Development Establishment: An Application of Aeroballistics Range Techniques to Models With Digonal Rotational Symmetry. B.R.L. Rep. 1005, Part 1, Proc. Aerodynamics Range Symposium, Jan. 1957.

2. Rhoads, D. W., and O'Hara, J. C.: Rolling Pullout Study - Part I. Development of a Large Disturbance Theory for Calculating Airplane Motions and Tail Loads in a Rolling Pullout Maneuver. Cornell Aero. Lab. Rep. TB-541-F-1, Apr. 1954.

3. Nielsen, Jack N., Kaattari, George E., and Anastasio, Robert F.: Lift and Center of Pressure of Wing-Body-Tail Combinations at Subsonic, Transonic, and Supersonic Speeds. NACA Rep. 1307, 1957.

4. Miles, J. W.: The Application of Unsteady Flow Theory to the Calculation of Dynamic Stability Derivatives. North American Aircraft Rep. No. AL-957, Sept. 8, 1950.

TABLE I.- MASS CHARACTERISTICS

Model	Weight grams	Center of gravity position, inches from nose	Moments of inertia, slug-ft^2		
			I_{XX}	I_{YY}	I_{ZZ}
8	138.97	3.36	9.46×10^{-6}	222.6×10^{-6}	229.9×10^{-6}
15	138.75	3.34	9.42×10^{-6}	223.1×10^{-6}	229.0×10^{-6}
16	139.53	3.35	9.51×10^{-6}	224.6×10^{-6}	230.4×10^{-6}

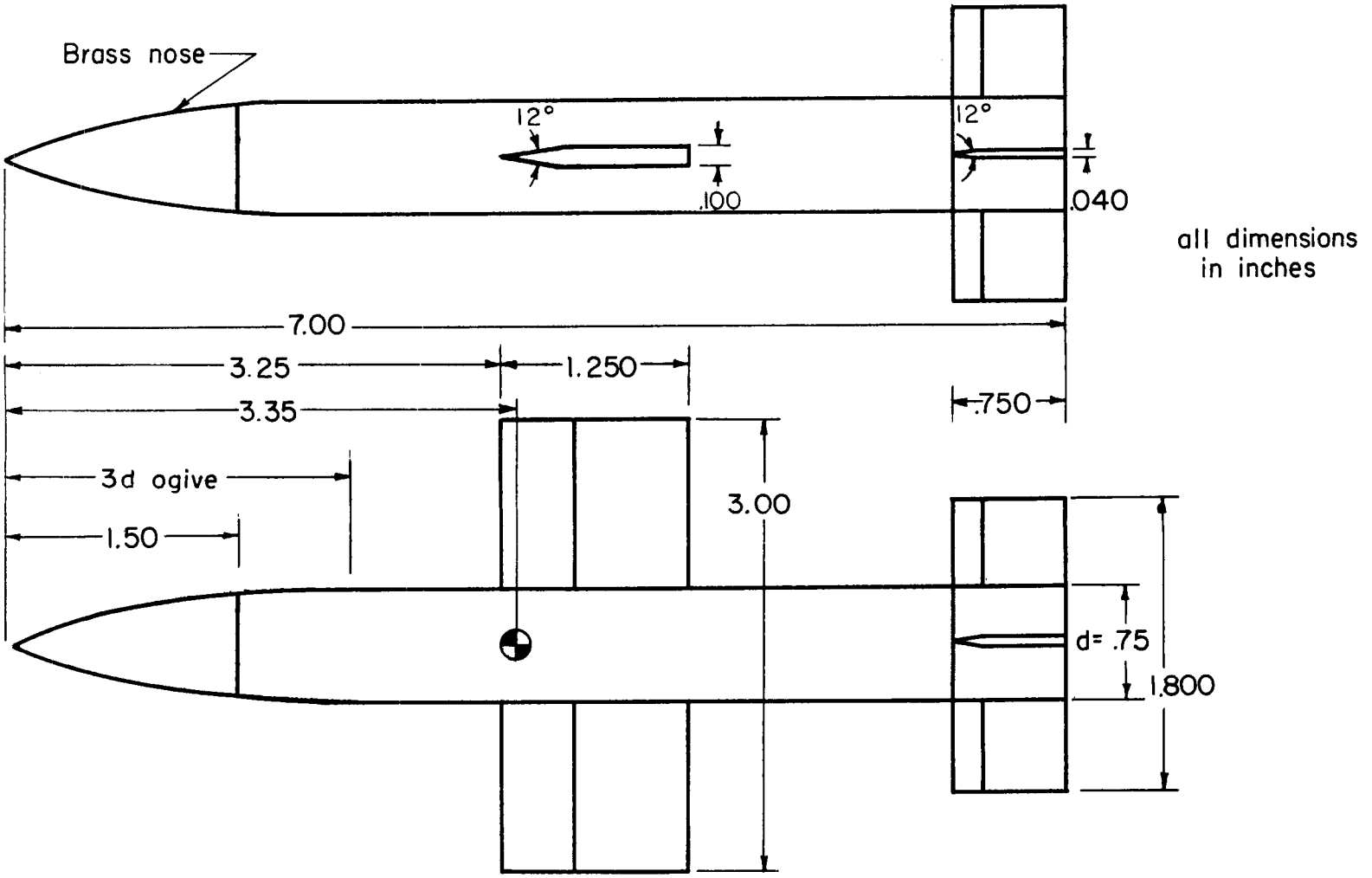

Figure 1.- Model.

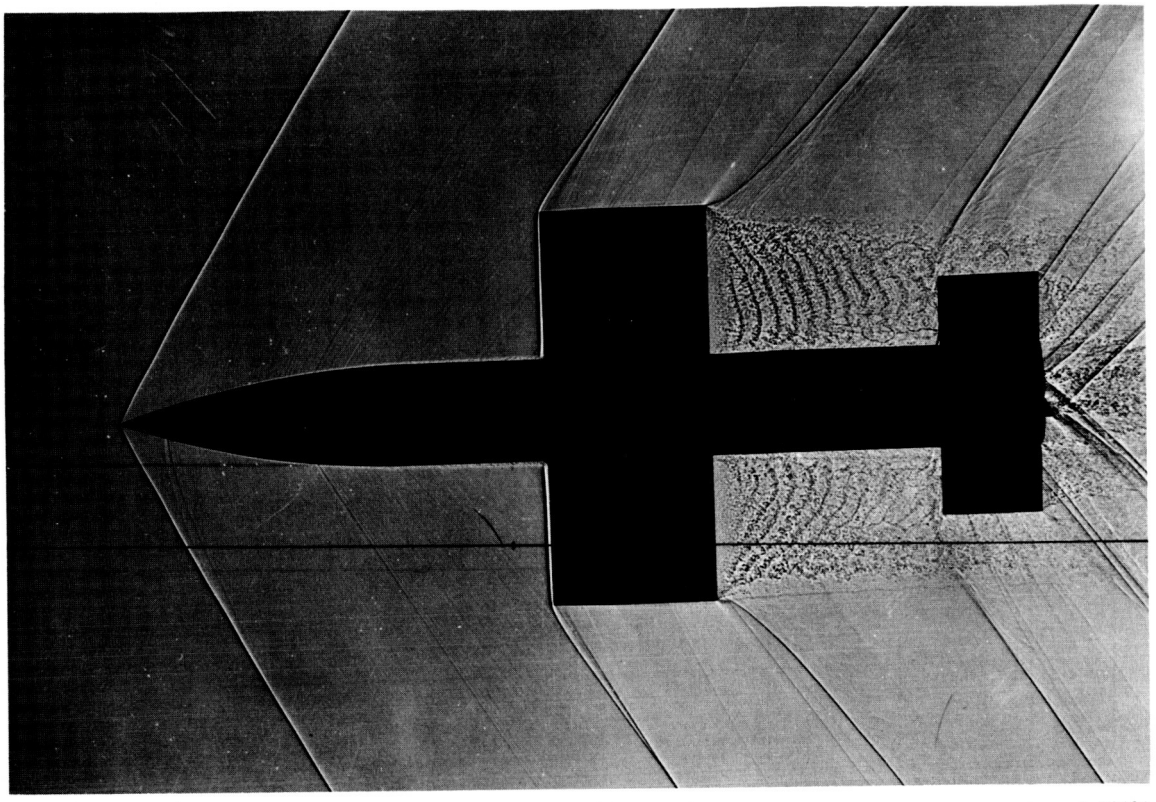

A-22494

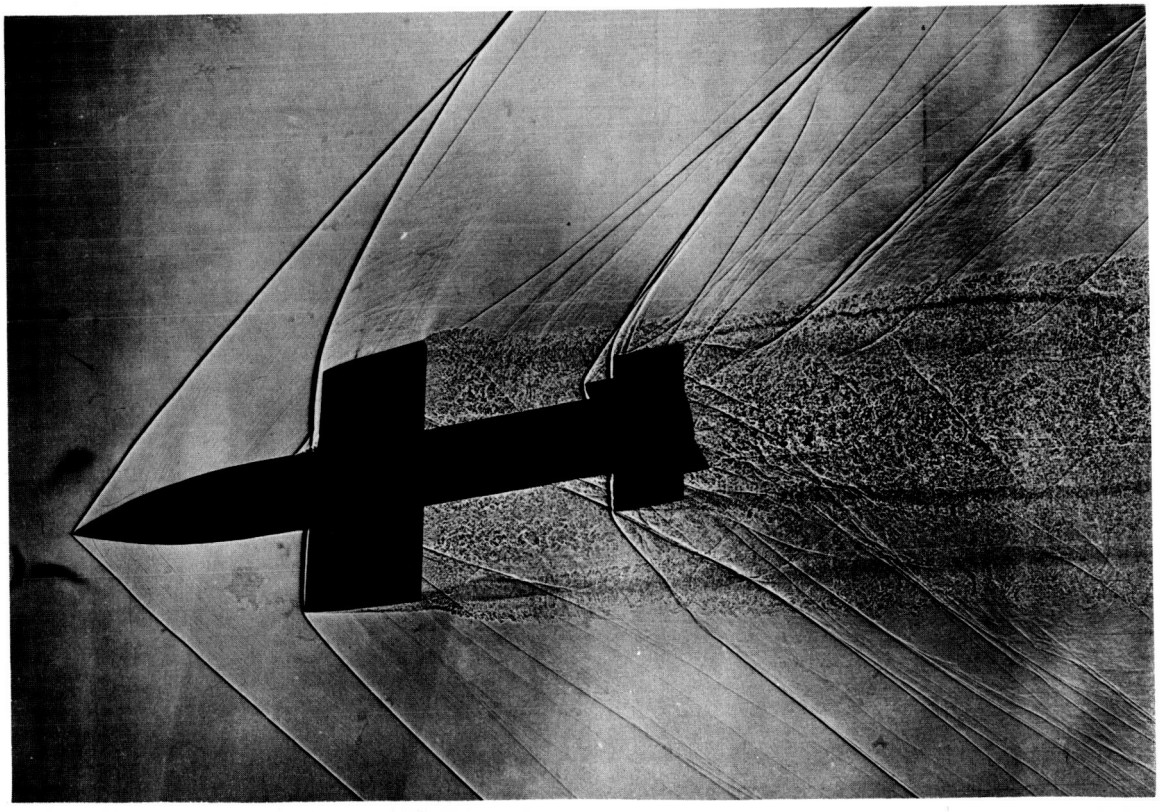

A-20400

Figure 2.- Shadowgraphs of models in flight.

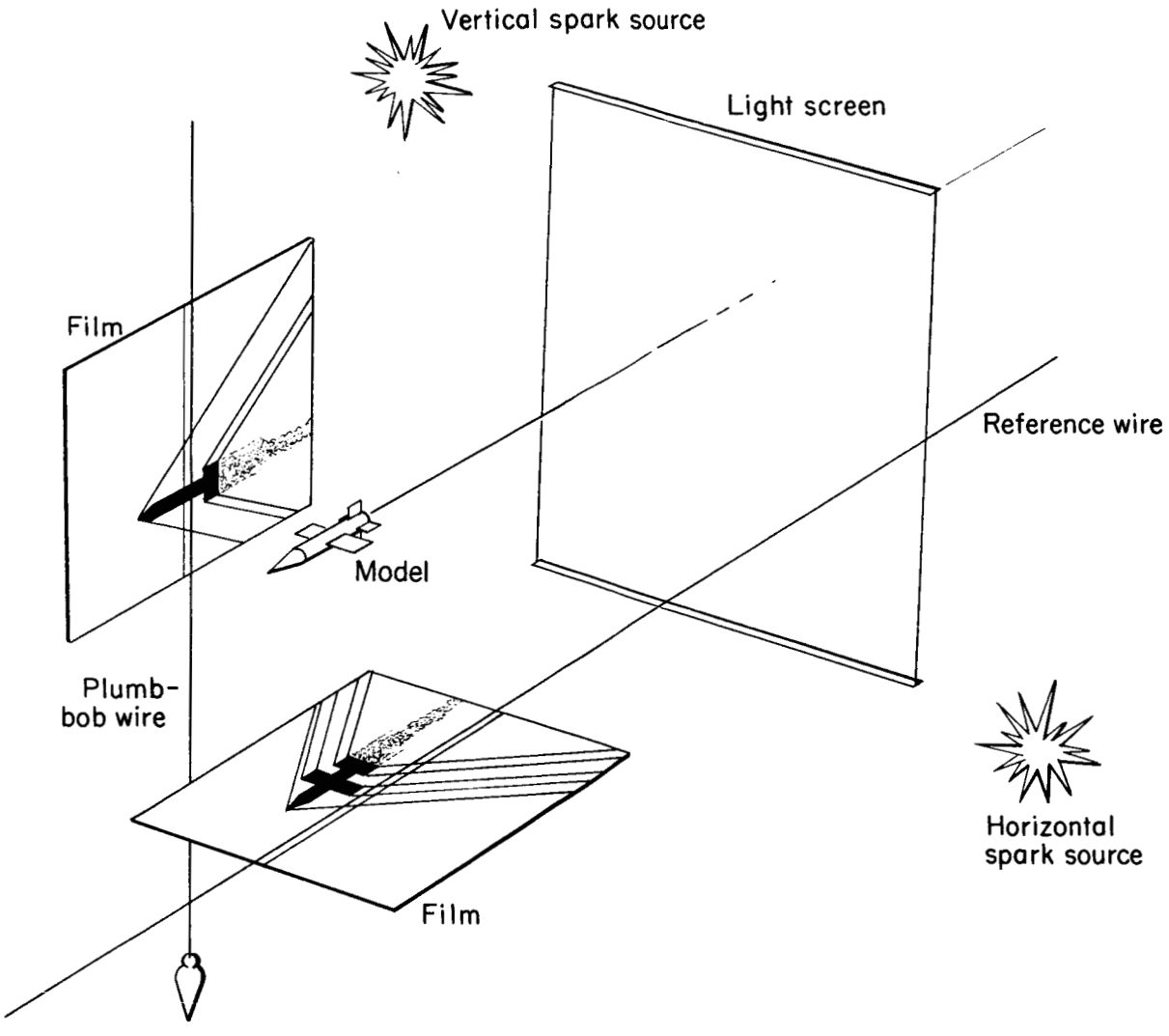

Figure 3.- Sketch of underground range station.

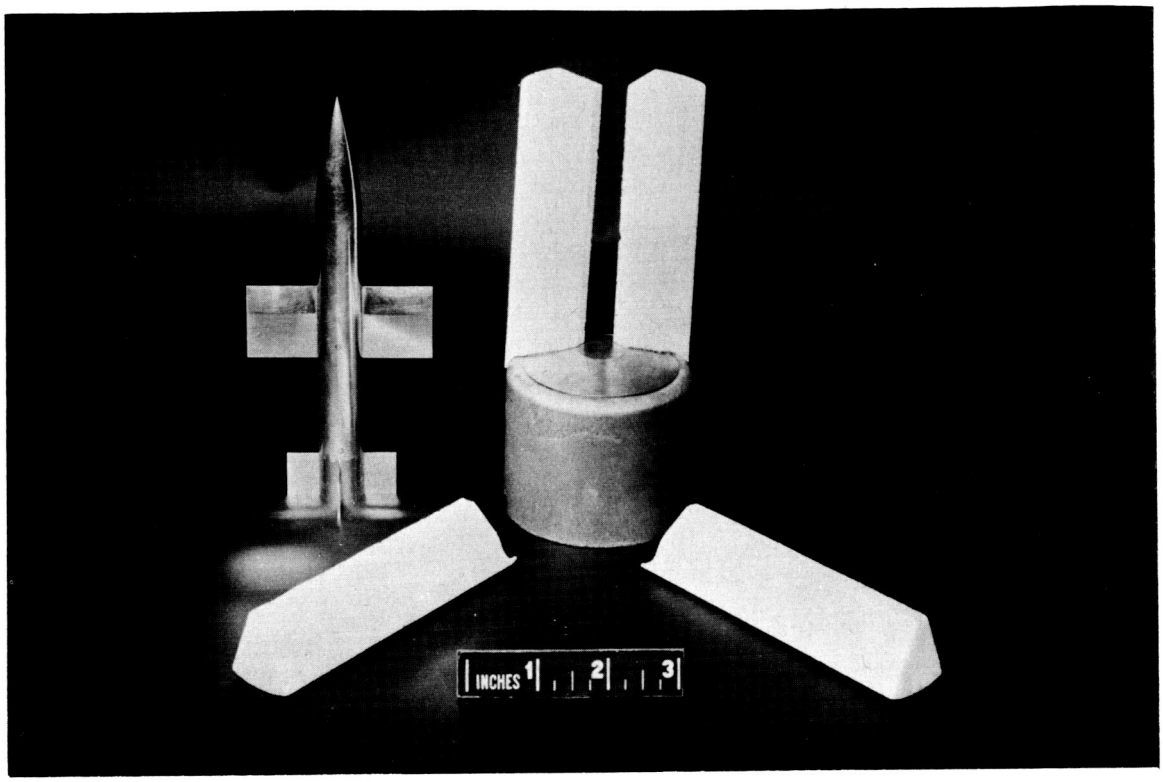

A-23039

Figure 4.- Photograph of model and sabot.

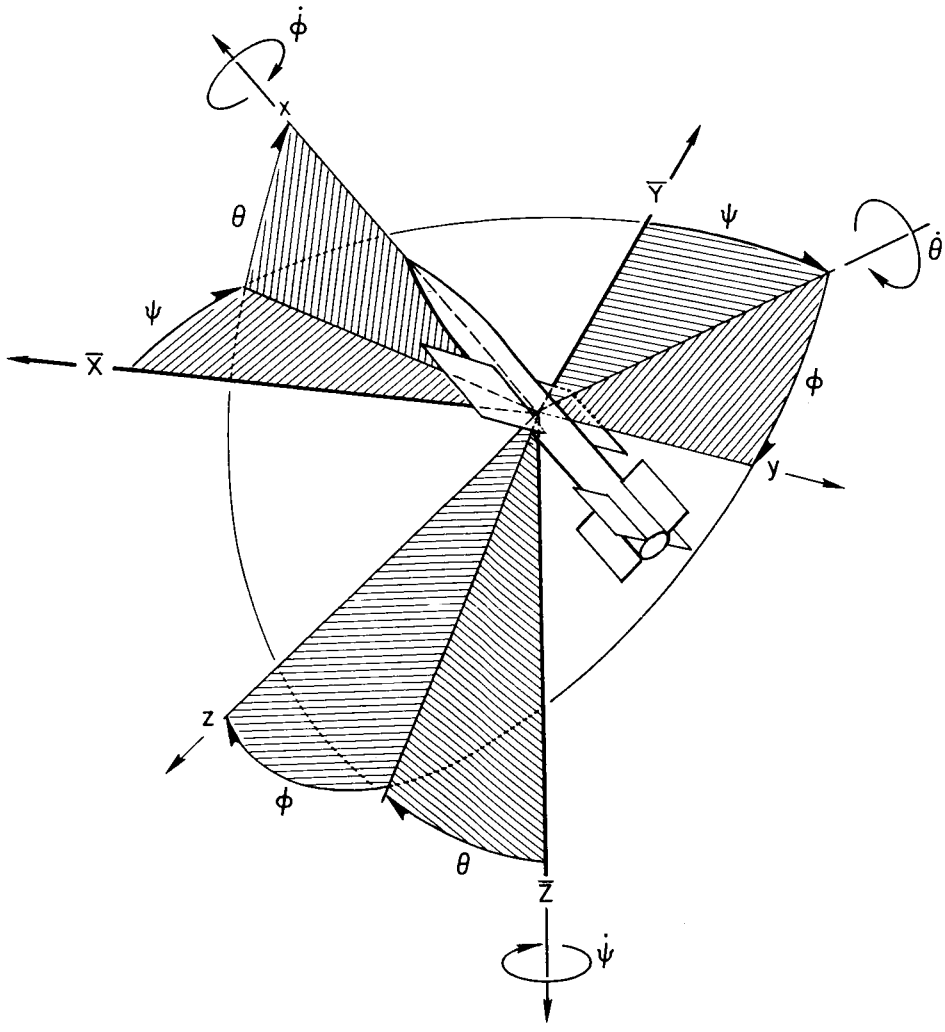

(a) Angular orientation of model axes with respect to earth fixed axes.

Figure 5.- Reference axes and angles.

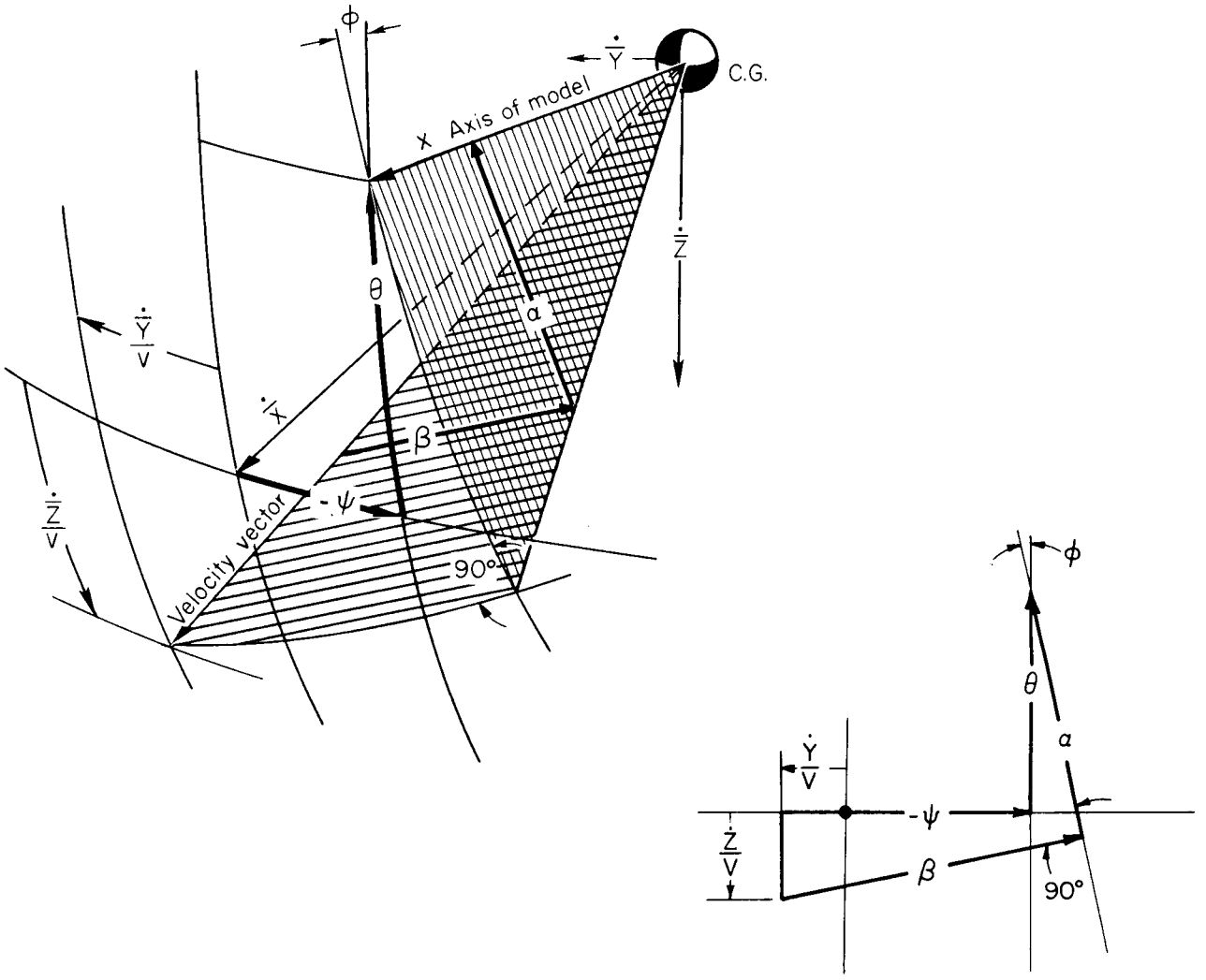

(b) Relationship of velocity vector and model axes in terms of orientation angles.

Figure 5.- Concluded.

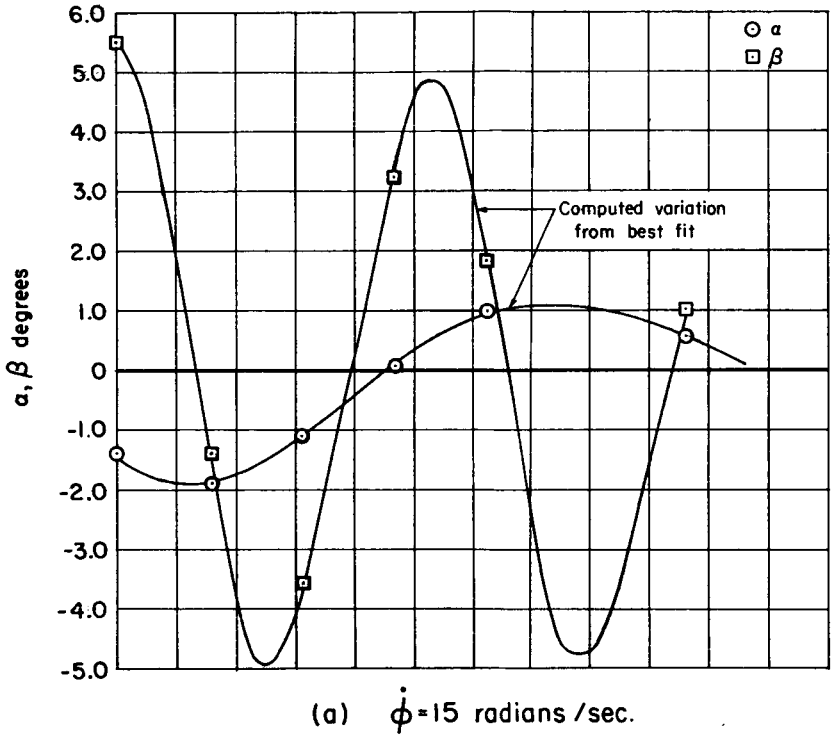

(a) $\dot{\phi}$ = 15 radians/sec.

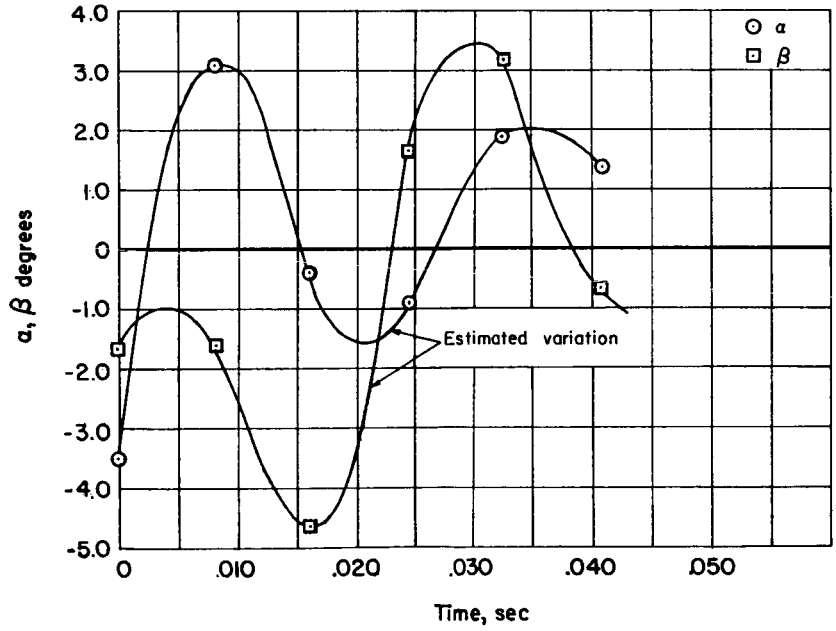

(b) $\dot{\phi}$ = 340 radians/sec.

Figure 6.- Excursions of α and β for rolling and nonrolling models.

$$-\ddot{\alpha} = A\dot{\alpha} + B\alpha + C\dot{\beta} + D\beta$$

$$-\ddot{\beta} = E\dot{\beta} + F\beta + G\dot{\alpha} + H\alpha$$

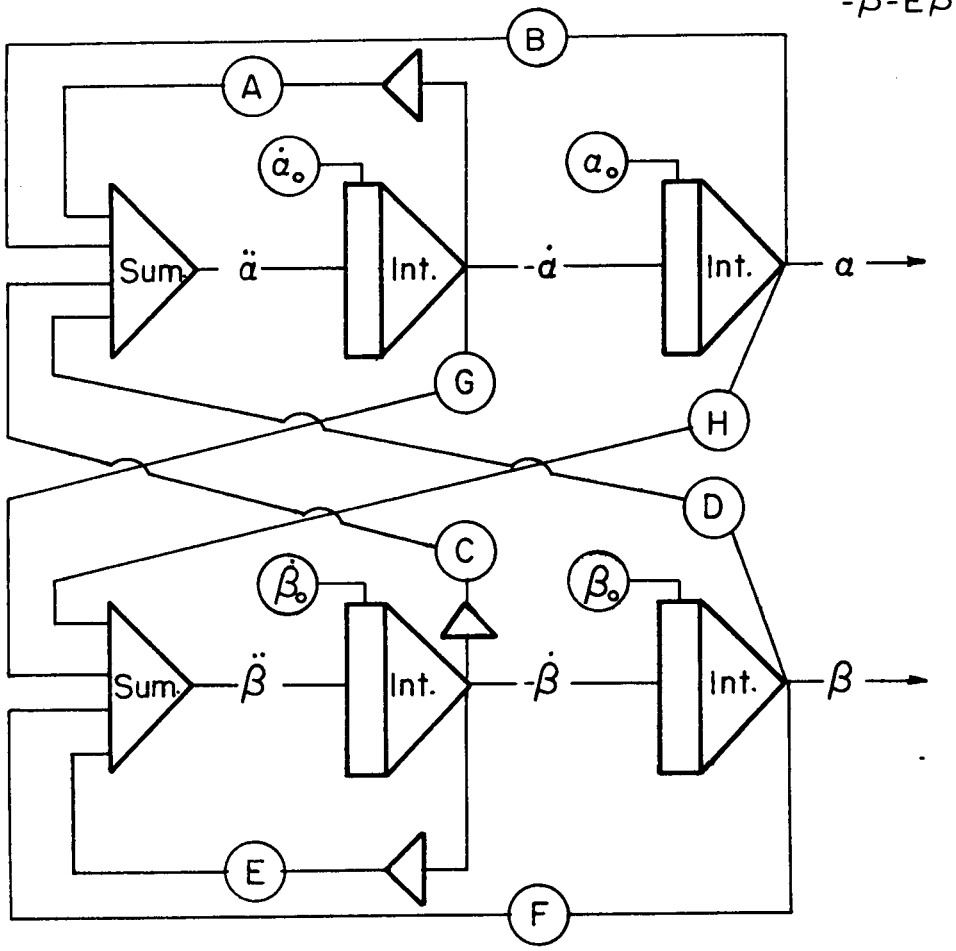

Figure 7.- Diagram of analog computer arrangement for coupled equations of motion.

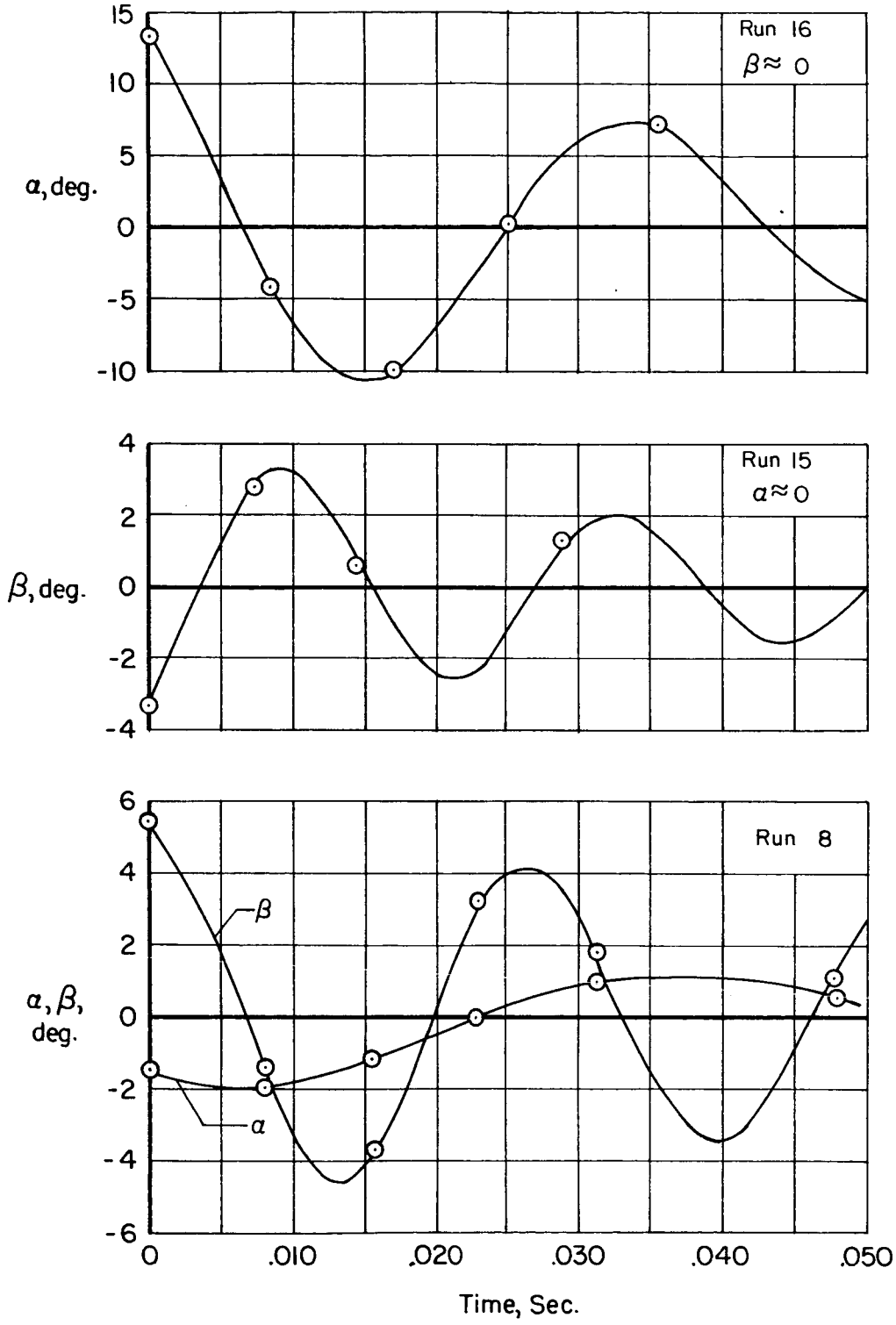

Figure 8.- Model trajectories for nonrolling flights.

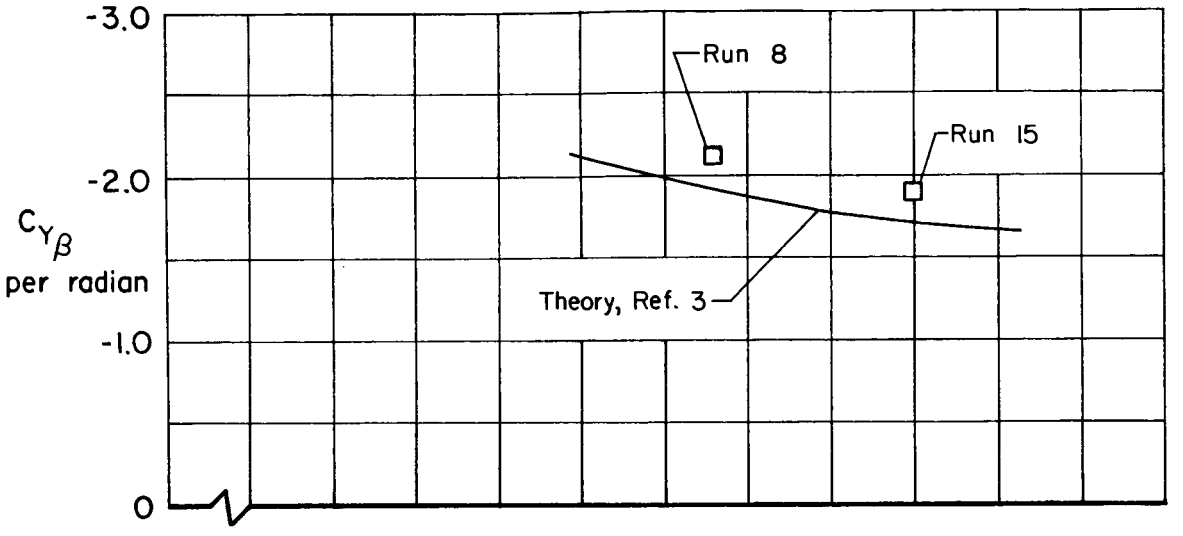

(a) Side-force curve slope vs. Mach number.

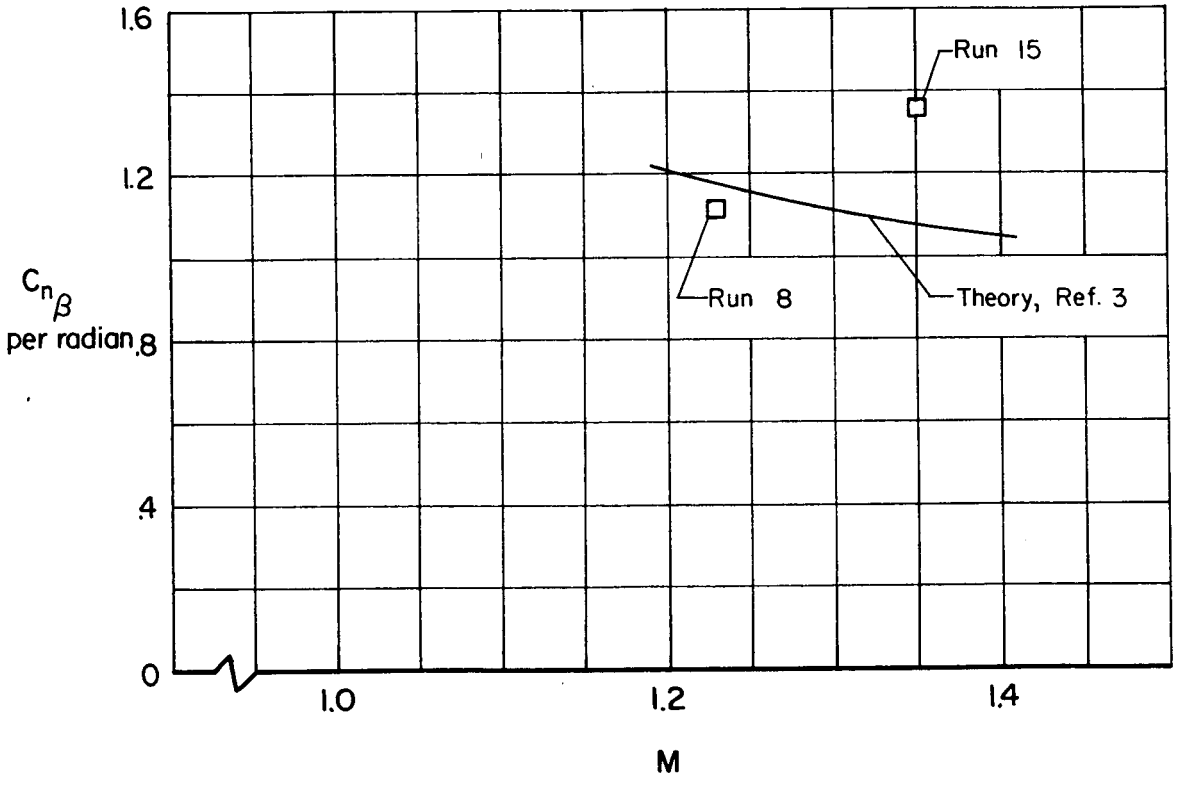

(b) Yawing-moment curve slope vs. Mach number.

Figure 9.- Lateral static derivatives.

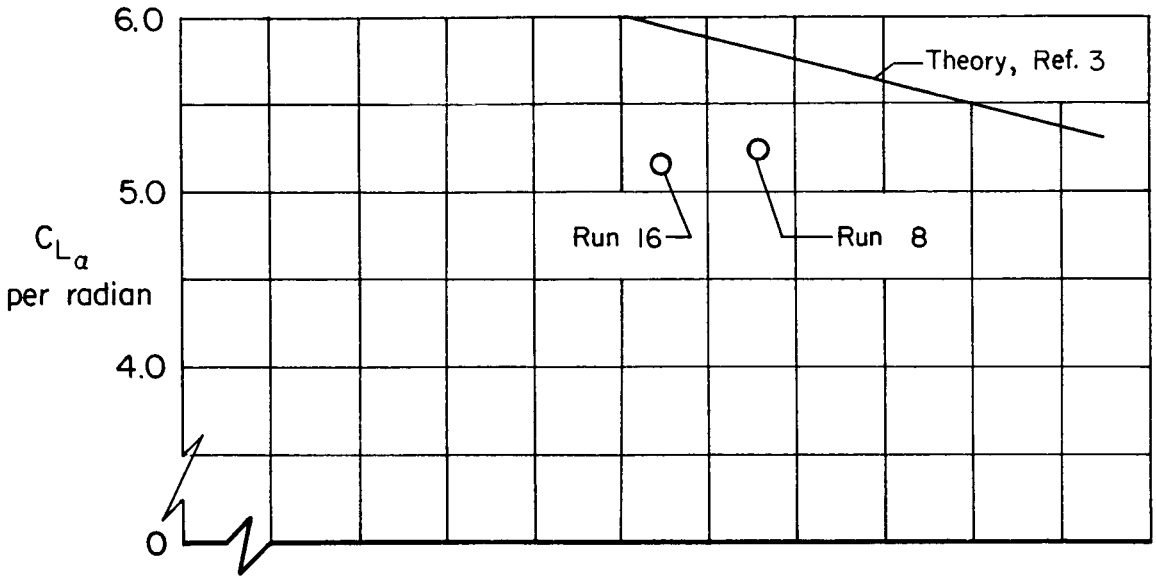

(a) Lift curve slope vs. Mach number.

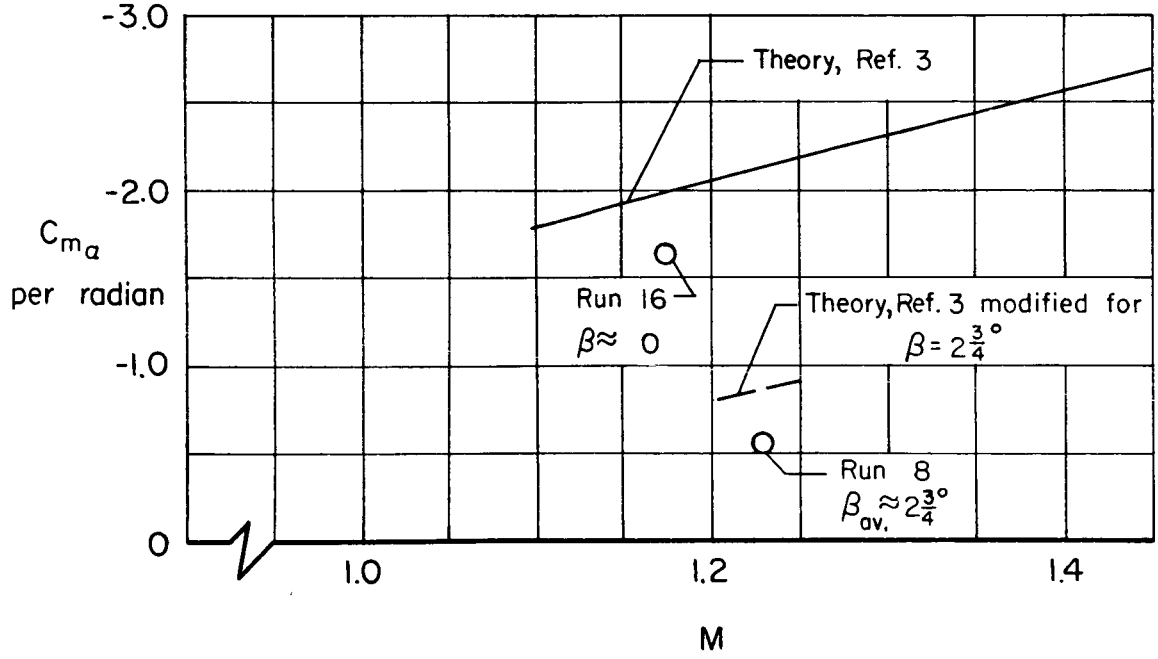

(b) Pitching-moment curve slope vs. Mach number.

Figure 10.- Longitudinal static derivatives.

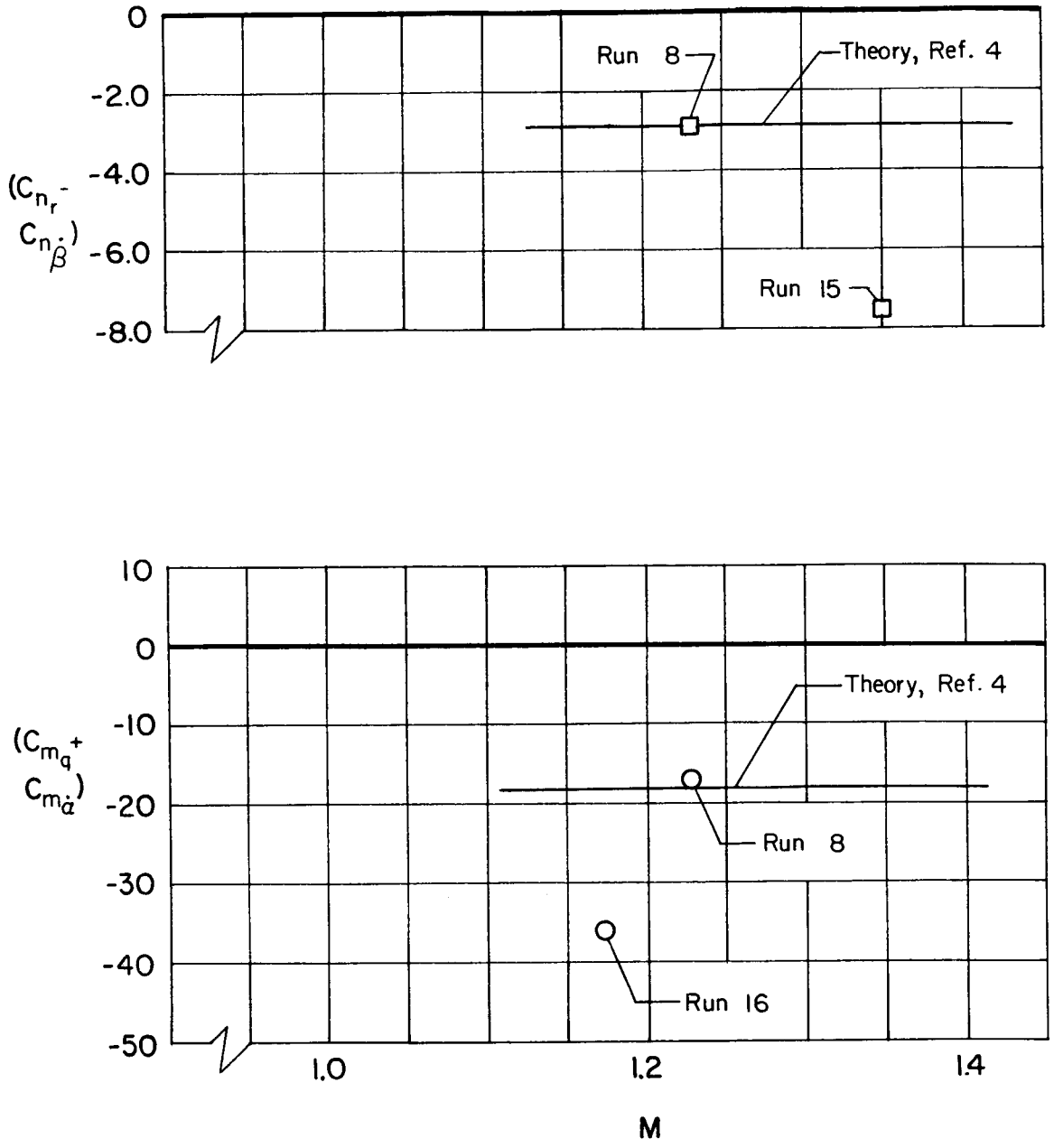

Figure 11.- Damping derivatives.

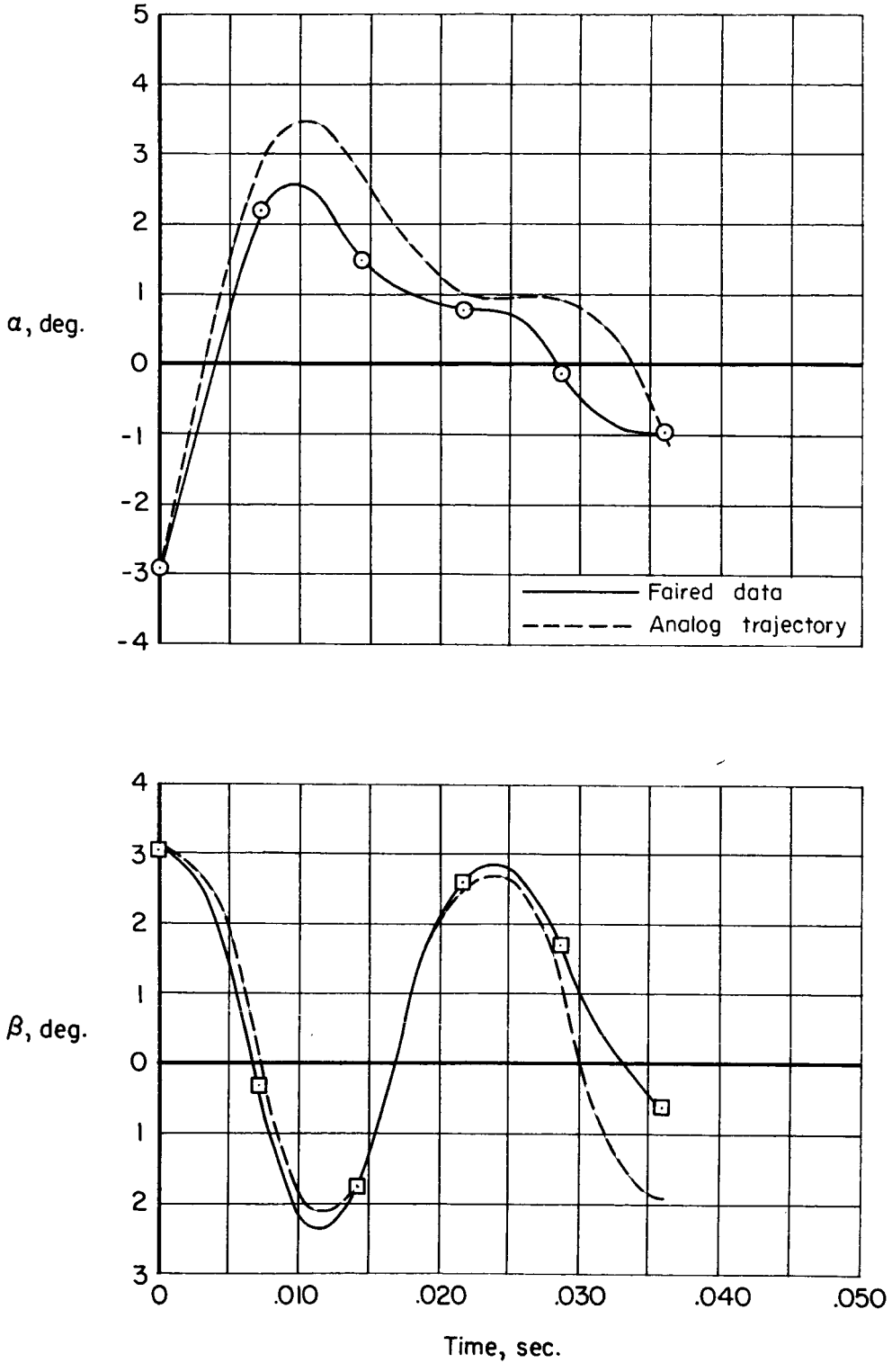

Figure 12.- Analog match to rolling flight.